THE TYRE AS A VEHICLE COMPONENT

HANS B. PACEJKA
DELFT UNIVERSITY OF TECHNOLOGY & TNO-DELFT
THE NETHERLANDS

ABSTRACT

The tyre force and moment generating properties connected with the vehicle's horizontal motions are considered. Knowledge of tyre properties is necessary to properly design vehicle components and advanced control systems. For this purpose, mathematical models of the tyre are being used in vehicle simulation models. In the paper, the simple brush tyre model is treated first to gain insight Then, the steady-state empirical 'Magic Formula tyre model' is discussed. A full description of the steady-state part of the new version 'Delft Tyre 96' is added. The non-steady state behaviour of the tyre is of importance in rapid transient maneuvres, when cornering on uneven roads and for the analysis of oscillatory braking and steering properties. A relatively simple model that is restricted to low time and path frequencies, based on the relaxation length concept, is introduced.

THE TYRE AS A FORCE AND MOMENT GENERATOR

In each of the three perpendicular directions the tyre is capable to generate forces. They are needed to carry the vehicle's weight, to steer and to brake or accelerate the vehicle. Apart from the forces, that is: the normal load F_z, the lateral cornering force F_y and the longitudinal driving or braking force F_x, the tyre produces moments about the corresponding axes. The aligning torque M_z acting about the vertical axis is the more important one. In Figure 1 these forces and moment acting from road to tyre have been indicated. Forces and moments are the result of tyre deflections that occur due to the mutual interaction between wheel and road. Obviously, the normal or radial deflection of the tyre is a direct result of the vertical motion of the wheel axle and the vertical profile of the road surface. The horizontal deflections of the tyre are connected with the horizontal and rotational motions of the wheel that may induce longitudinal and lateral slip of the wheel with respect to the ground.

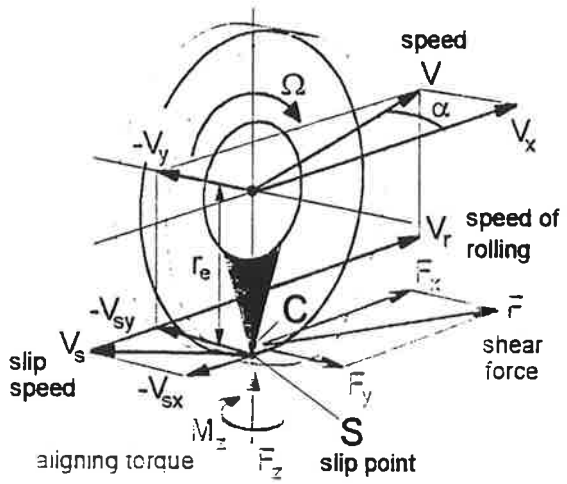

Figure 1 Tyre forces and moment generated through tyre deflections and wheel slip velocities.

To become more precise, it is useful to introduce the so-called slip point S. This imaginary point is attached to the wheel rim and at the instant of observation the point is located in the lowest position, that is on the radius passing through the so-called contact centre or point of intersection C. This latter point forms the intersection of three planes: the road plane, the wheel centre plane and the plane passing through the wheel spin axis and perpendicular to the road plane. The slip point S is normally located slightly below the road surface. Its distance to the wheel centre is defined as the slip radius r_s. Here, we take the slip radius equal to the so-called effective free rolling radius r_e. The horizontal velocity of the slip point is the slip speed of the wheel (rim) with respect to the road. Apparently, at free rolling (no driving or braking torque) the longitudinal component of the slip velocity equals zero. When the wheel is being braked, point S moves in forward direction with longitudinal slip speed V_{sx}. When the slip point moves sideways, a lateral slip velocity V_{sy} arises. Note that the difference between lateral velocities of points S and C may be neglected. The resulting velocity V_s of point S represents the vector of the slip speed of the wheel.The slip speed components may be used directly to determine the resulting forces and moment. In practice, however, it appears in most cases to be more practical to use the components of the wheel slip vector as input quantities. These slip quantities are obtained by dividing the slip speed components by the forward speed V_x of the wheel centre (or better: of the contact centre C).

$$\kappa = -\frac{V_{sx}}{V_x} \tag{1}$$

$$\tan\alpha = -\frac{V_{sy}}{V_x} \tag{2}$$

Here, α is the slip angle as indicated in Figure 1. Other conventions may define different signs and symbols. Currently, a debate is going as to whether the longitudinal slip κ should be defined such that it equals zero at free rolling (as adopted here) or at vanishing longitudinal force F_x=0. As a consequence, in the latter case a slightly shorter value of the slip radius results. The first definition is often used because of traditional testing procedures. The latter has the advantage that it can still be used even on very slippery surfaces where free rolling might not occur due to the low friction level not being able to overcome the tyre rolling resistance.

The slip components α and κ together with spin slip due to wheel camber and possibly turn slip (path curvature) may serve as input quantities in a tyre model. With such a mathematical model the resulting forces and moments can be calculated. The normal load and possibly the speed of travel are used as service parameters.

TYRE MODELLING

Tyre models are used to calculate the tyre forces and moment as responses to the wheel motion that may be given in terms of the various slip quantities. We may distinguish theoretical models based on physics of the tyre construction, and empirical models which are solely based on experimental findings. Also, combinations of both approaches are used in the development of the tyre model.

The models that are in use nowadays range from very simple to highly complex descriptions of tyre behaviour. The model becomes more complex when we need to consider:

- larger magnitudes of wheel slip, requiring a non-linear description
- combined slip as opposed to pure lateral or pure longitudinal slip

- wheel camber and turn slip
- wet or icy roads which makes the friction coefficient dependency on speed no longer negligible
- time-varying wheel motion which requires a non-steady-state / transient tyre model development
- high frequency inputs and high speed of travel necessitating the inclusion of tyre inertial properties
- short wavelength wheel oscillations and road irregularities requiring more detailed contact line considerations
- simulations starting from or ending at stand-still

To start the overview of some cathegories of tyre modelling and tyre dynamic behaviour, we will first treat the relatively simple case of steady-state wheel slipping motions over a flat level road surface.

SIMPLE STEADY-STATE SLIP CONSIDERATIONS

In the state-of-the-art paper [1] a description is given of recent tyre models. The discussion was restricted to those models that were developed for use in vehicle dynamics studies at or close to steady-state conditions. To gain insight, let us first consider a very simple physical model that can nicely explain how the forces and the moment are generated through the action of wheel slip in pure lateral or longitudinal directions or at a combination of these slip components (e.g. braking in a curve).

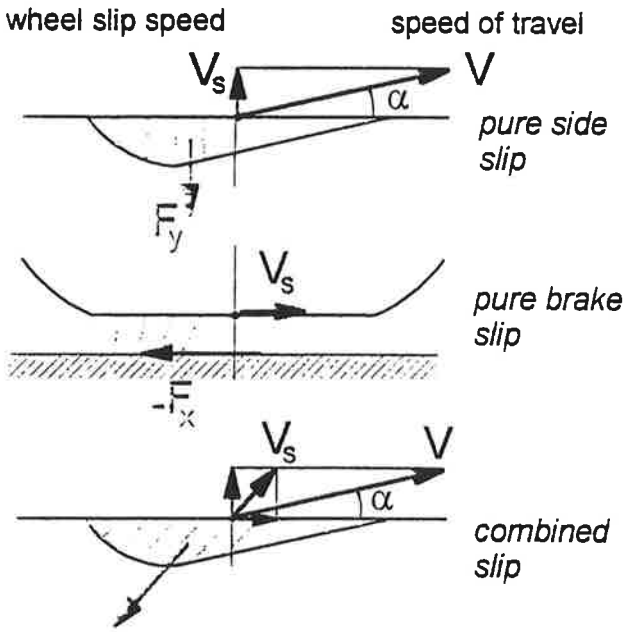

Fig. 2 Three modes of slip of the brush tyre model.

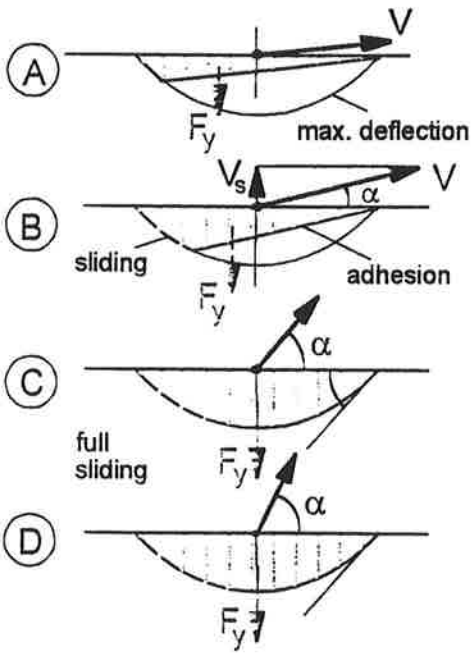

Fig. 3 The brush model at different levels of side slip.

The model is the so-called brush tyre model. The elastic bristles (similar to tread elements) are attached to the rim or to the assumedly rigid carcass (can only deflect vertically to accommodate the flat contact area). In the contact zone, the other ends of the bristles touch the road surface. Figure 2 depicts the deflected brush model. Three different cases of slip are considered. For each case the wheel slip speed vector (that is the speed of point *S* of the actual wheel) has been indicated. The base points of the elastic elements move parallel with respect to

the road with that slip speed V_s (turn slip and camber not considered). As soon as the foremost element (at the right hand side of the diagram) touches the road, the deformation starts to develop. The end point of the element that touches the surface remains in contact without sliding upto a point along the contact line where the frictional force that is maximally available, is not enough to further deflect the element. At that transition point, the sliding zone is entered. In that zone, the element will continue to slide until it is lifted from the ground at the trailing edge. It may be noted that in the adhesion zone, where sliding does not occur, the contact line is straight and parallel to the speed vector of the wheel centre (or better: of the contact centre C).

The model is simplified in that the friction coefficient is assumed to be constant (Coulomb friction) and that the horizontal stiffness of the elements are assumed the same in all directions. Further, a symmetric parabolic pressure distribution is considered. For the case of pure lateral slip, Figure 3 shows how the deflection changes in magnitude and in distribution when the slip angle increases from very small to large. The initially approximately triangular shape (due to almost vanishing sliding) changes into a symmetric distribution when complete sliding is reached (case C).

We observe that the side force increases and that at the same time the pneumatic trail (the moment arm of the side force) decreases with increasing side slip. The resulting characteristics for the side force F_y and the aligning torque M_z are presented in Figure 4. From the slip angle where complete sliding starts (case C), the side force is saturated and attains its maximum value equal to the friction coefficient μ times the vertical load F_z while the moment becomes equal to zero. The curves appear to be very similar in nature to those established from measured data.

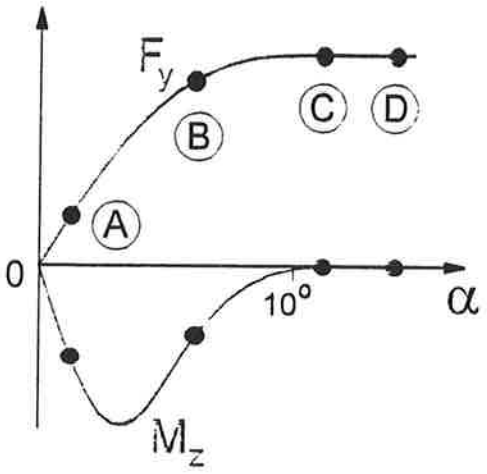

Fig. 4 The resulting side force and aligning torque characteristics of the model of Figure 3 with the corresponding cases A, B, C and D indicated.

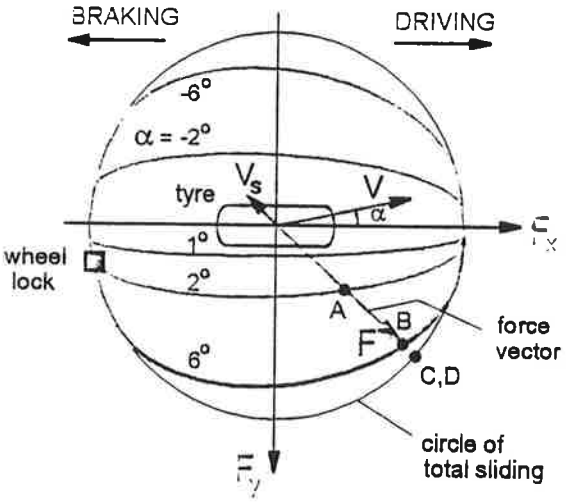

Fig. 5 Combined slip characteristics for the side force versus fore and aft force at constant values of the slip angle. Cases A, B, C and D of this isotropic tyre model correspond in level of total slip with those indicated in Figures 3 and 4.

Sometimes, a different kind of characteristic is made: the so-called Gough plot.Then, the side force is plotted versus the aligning torque. Along the curve the slip angle changes. For larger value of the friction coefficient the curves tend to spread in radial direction. When such a collection of curves is available for an actual tyre measured on surfaces with different levels of friction, the friction coefficient may be estimated when on the road the side force and the aligning torque are measured and the value of the vertical load is available as well. We refer to [2] where this principle is adopted to use the tyre as a friction sensor without having the need to measure the slip angle. The case of combined slip (bottom diagram of Figure 2) is analogous to the cases of pure lateral or longitudinal slip. Figure 5 shows the resulting F_y vs F_x diagram. Along the curves for constant slip angle α the longitudinal slip κ varies. For a given ratio of $\tan\alpha$ and κ, that is for a given direction of the slip speed vector V_s (and the opposite to that directed force vector F) the four cases of increasing resulting slip A, B, C, and D have been indicated again.

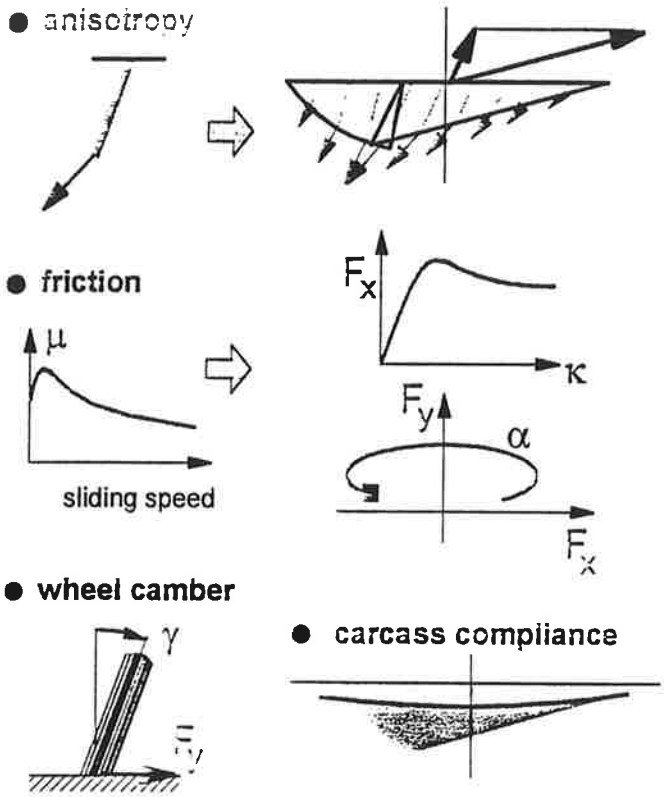

Figure 6 Physical factors that complicate modelling of the tyre.

Although the diagrams appear quite realistic, this simple brush model is in general not suitable to produce quantitatively correct and thus acceptable results. Considerable deviations may occur and the following important features which are not included in the simple brush model may be responsible for these (cf. Figure 6): unequal stiffnesses in x and y directions, non-constant friction coefficient, lateral compliance of the carcass and belt, non-symmetric and non-constant pressure distribution. Introducing these factors in a tyre model would considerably increase its complexity. Also, the introduction of wheel camber and turn slip would complicate the matter. An alternative way to achieve a better mathematical description is the use of an empirical model.

A CONSISTENT MAGIC FORMULA TYRE MODEL

A widely used empirical tyre model is based on the so-called Magic Formula. The development of the model was started in the mid-eighties. In a cooperative effort TU-Delft and Volvo developed several versions (1987, 1989, 1991). In these models the combined slip situation was modelled from a physical view point. In 1993 Michelin introduced a purely empirical method using Magic Formula based functions to describe the tyre horizontal force generation at combined slip. This approach was adopted by DVR (joint venture of TU-Delft and TNO- Delft). In the newest version (Delft Tyre 96) the original description of the aligning torque is altered to accommodate a relatively simple combined slip extension. The pneumatic trail is introduced as a basis to calculate this moment about the vertical axis. A complete description of the model is given in the Appendix.

We refer to [3] for a detailed treatment of the pure slip part of this model (that is: either lateral or longitudinal slip). For the side force and the fore and aft force that part of the model remained unchanged. The formula reads:

$$y = D \sin[C \arctan\{Bx - E(Bx - \arctan Bx)\}] \tag{3}$$

with

$$\begin{aligned} Y(X) &= y(x) + S_v \\ x &= X + S_h \end{aligned} \tag{4}$$

where

- Y: output variable F_x or F_y
- X: input variable α or κ

and

- B: stiffness factor
- C: shape factor
- D: peak value
- E: curvature factor
- S_h: horizontal shift
- S_v: vertical shift

The Magic Formula $y(x)$ typically produces a curve that passes through the origin $x=y=0$, reaches a maximum and subsequently tends to a horizontal asymptote. For given values of the coefficients B, C, D and E the curve shows an anti-symmetric shape with respect to the origin. To allow the curve to have an off-set with respect to the origin two shifts S_h and S_v have been introduced. A new set of coordinates $Y(X)$ arises as shown in Figure 7. The formula is capable of producing characteristics that closely match measured curves for the side force F_y and the fore and aft force F_x as functions of their respective slip quantities: slip angle α and longitudinal slip κ.

Figure 7 (upper part) illustrates the meaning of some of the factors with the help of a typical side force characteristic. Obviously, coefficient D represents the peak value (with respect to the x-axis) and the product BCD corresponds to the slope at the origin (x=y=0). The shape factor C controls the limits of the range of the sine function appearing in the formula (3) and thereby determines the shape of the resulting curve. The factor B is left to determine the slope at the origin and is called the stiffness factor. The offsets S_h and S_v appear to occur

when ply-steer and conicity effects and possibly the rolling resistance cause the F_y and F_x curves not to pass through the origin. Also, wheel camber will give rise to a considerable offset of the F_y vs α curves. Such a shift may be accompanied by a significant deviation from the pure anti-symmetric shape of the original curve. To accommodate such an asymmetry, the curvature factor E is made dependent of the sign of the abscissa (x).

$$E = E_o + \Delta E \cdot \mathrm{sgn}(x) \tag{5}$$

Also the difference in shape that is expected to occur in the F_x vs κ characteristic between the driving and braking ranges can be taken care of.

The various factors are given functions of normal load and wheel camber angle. A number of parameters appears in these functions. A suitable regression technique is used to determine their values from measured data corresponding to the best fit (cf. [4]). One of the important functional relationships used is the variation of the cornering stiffness (or approximately: $BCD_y = \partial F_y / \partial \alpha$ at $\alpha + S_h = 0$) with F_z.

$$BCD_y = p_1 \sin[2 \arctan(F_z/p_2)] \cdot (1 - p_3|\gamma|) \tag{6}$$

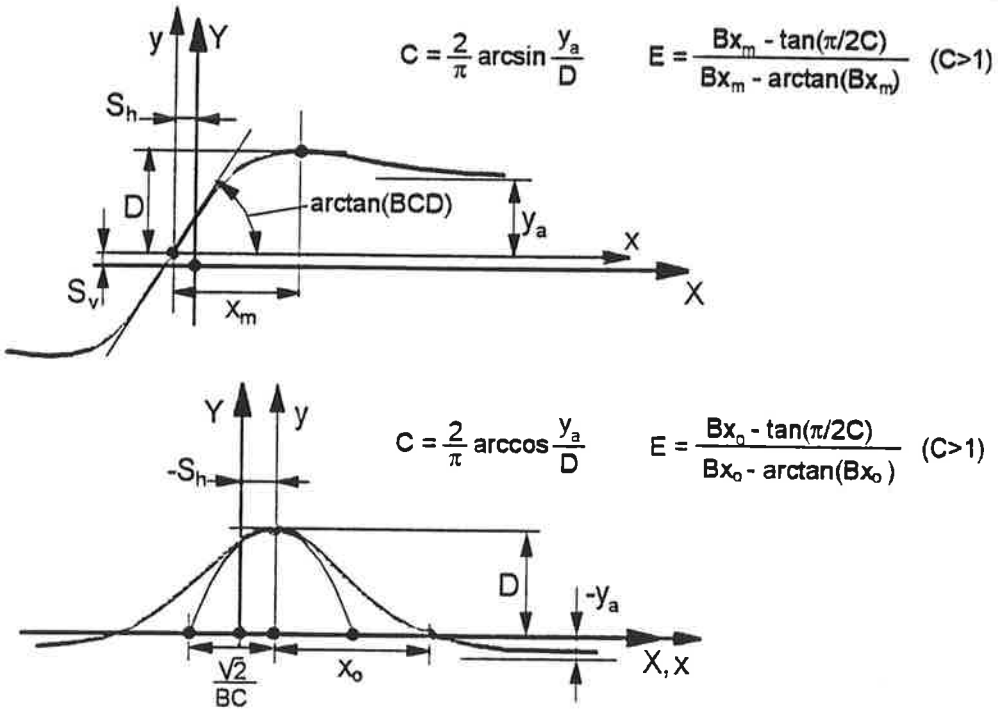

Figure 7 Curves produced by the sine and cosine versions of the Magic Formula, Eqs.(3) and (8). Meaning of curve parameters have been indicated.

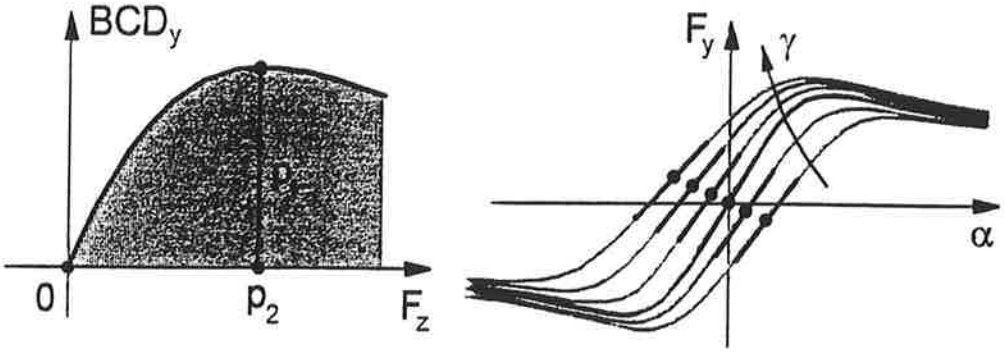

Figure 8 Cornering stiffness versus vertical load and the influence of wheel camber, Eq. (6).

For zero camber, the cornering stiffness attains its maximum p_1 at $F_z=p_2$. In Figure 8 the basic relationship has been depicted. Apparently, for a cambered wheel the cornering stiffness is decreased.

The aligning torque M_z can now be obtained by multiplying the side force F_y with the pneumatic trail t and adding the usually small residual torque M_{zr} (Figure 9). We have:

$$M_z = -t \cdot F_y + M_{zr} \tag{7}$$

with the pneumatic trail

$$t(\alpha_t) = D_t \cos[C_t \arctan\{B_t\alpha_t - E_t(B_t\alpha_t - \arctan(B_t\alpha_t))\}] \tag{8}$$

$$\alpha_t = \alpha + S_{Ht} \tag{9}$$

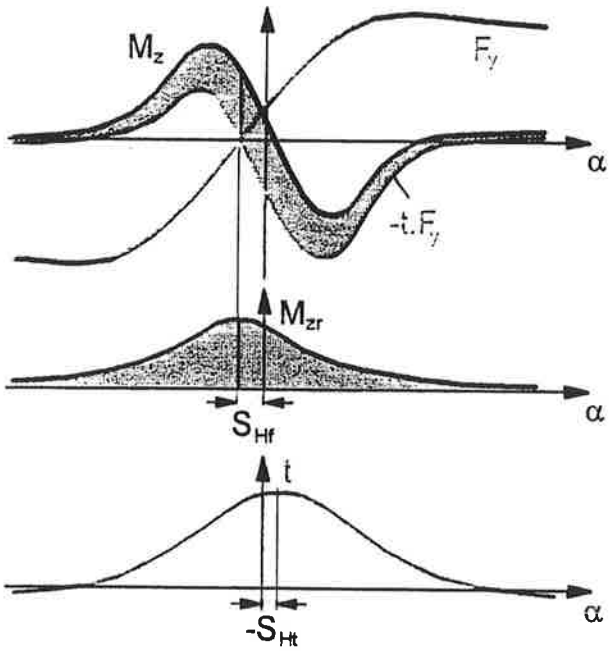

Figure 9 Aligning torque characteristic produced by adding two parts: the product of side force and pneumatic trail and the residual torque, Eq. (7) .

and the residual torque:

$$M_{zr}(\alpha_r) = D_r \cos[\arctan(B_r \alpha_r)] \tag{10}$$

$$\alpha_r = \alpha + S_{Hf} \tag{11}$$

It is seen that both parts of the moment are modelled using the Magic Formula, but instead of the sine function, the cosine function is employed. In that way a hill-shaped curve is produced.

In Figure 7 (lower part) the basic properties of the cosine M.F. curve have been indicated (subscripts of factors deleted). Again, D is the peak value, C is a shape factor determining the level of the horizontal asymptote and now B influences the curvature at the peak (illustrated with the parabola). Factor E changes the shape at larger values of slip. The residual torque attains its maximum D_r at the slip angle where the side force becomes equal to zero. This is accomplished through the horizontal shift S_{Hf}. The peak of the pneumatic trail occurs at $\alpha = -S_{Hf}$. This formulation has proven to give excellent agreement with measured curves. The advantage with respect to the earlier versions where formula (3) is used for the aligning torque as well, is that we have now directly assessed the pneumatic trail which is needed (as in the previous version [3]) for handling the combined slip situation.

In [3] the tyre's response to combined slip was modelled by using physically based formulae. A newer more efficient way is purely empiric. This method was developed by Michelin and published in [5]. It describes the effect of combined slip on both the lateral and the longitudinal forces. Weighting functions G are introduced which when multiplied with the original pure slip functions (that is Eq.(3)) produce the interactive effects of κ on F_y and of α on F_x. The weighting functions have a hill shape. They should take the value one in the special case of pure slip (κ or α equal to zero). When, for example, at a given slip angle a from zero increasing brake slip is introduced, the relevant weighting function for F_y may first show a slight increase in magnitude (becoming larger than one) but will soon reach its peak after which a continuous decrease follows. The cosine version of the Magic Formula is used to represent the hill shaped function:

$$G = D \cos[C \arctan(Bx)] \tag{12}$$

Here, G is the resulting weighting factor and x is either κ or α (possibly shifted). The coefficient D represents the peak value (slightly deviating from one if a horizontal shift of the hill occurs), C determines the height of the hill's base and B influences the sharpness of the hill. Apparently, the factor E was not needed to improve the fit. For the side force we get the following formulae:

$$F_y = G_{y\kappa} \cdot F_{yo} + S_{Vy\kappa} \tag{13}$$

$$G_{y\kappa} = \frac{\cos[C_{y\kappa} \arctan\{B_{y\kappa}(\kappa + S_{Hy\kappa})\}]}{\cos[C_{y\kappa} \arctan(B_{y\kappa} S_{Hy\kappa})]} \tag{14}$$

$$B_{y\kappa} = r_{By1} \cos[\arctan\{r_{By2}(\alpha - r_{By3})\}] \tag{15}$$

$$S_{Vy\kappa} = D_{Vy\kappa} \sin[r_{Vy5} \arctan(r_{Vy6} \kappa)] \tag{16}$$

In Eq.(13) F_{yo} denotes the side force at pure side slip obtained from Eq.(3); $S_{Vy\kappa}$ is the vertical shift sometimes referred to as the κ-induced ply-steer. This function varies with longitudinal slip κ as indicated in (16). Its maximum $D_{Vy\kappa}$ decreases with increasing magnitude of the slip angle (cf. App.). The factor $B_{y\kappa}$ influences the sharpness of the hill shaped weighting function (14). As indicated, the hill becomes more shallow (wider) at larger slip angles (then $B_{y\kappa}$ decreases according to (15)). The other coefficients appearing in the formulae are treated as constants. The combined slip relations for F_x are similar. However, a vertical shift was not needed to be included. In Figure 10 a three-dimensional graph is shown indicating the variation of F_x and F_y with both α and κ.

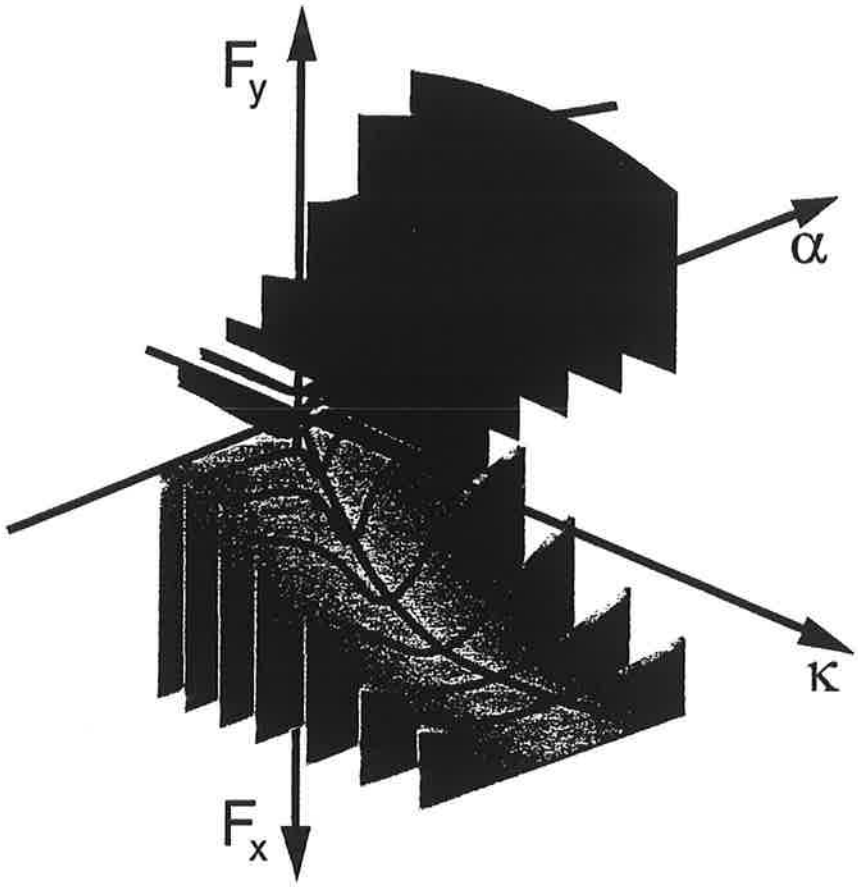

Figure 10 Combined slip lateral and longitudinal force 3-D diagrams showing the interaction of both slip components, Eqs. (13, 57, 62).

Regarding the aligning torque, physical insight is employed to model the situation at combined slip. The arguments α_t and α_r (including a shift) appearing in the functions for pneumatic trail and residual torque are replaced by equivalent slip angles incorporating the effect of κ on the composite slip. Besides, an extra term is included to account for the fact that an additional moment arm s arises for F_x as a result of camber γ and lateral tyre deflections through F_y (similar to the model description of [3]). The latter fact may give rise to a sign change

of the aligning torque in the range of braking.

$$M_z = -t(\alpha_{t,eq})\cdot F_y + M_{zr}(\alpha_{r,eq}) + s(F_y,\gamma)\cdot F_x \tag{17}$$

$$\alpha_{t,eq} = \arctan\sqrt{\tan^2\alpha_t + \left(\frac{K_x}{K_y}\right)^2 \kappa^2}\cdot \mathrm{sgn}(\alpha_t) \tag{18}$$

and similar for $\alpha_{r,eq}$. As mentioned before, the complete set of steady-state formulae has been listed in the Appendix. Parameters *p, q, r* and *s* of the model are non-dimensional quantities. In addition, user scaling factors λ have been introduced. With that tool the effect of changing friction coefficient, cornering stiffness, camber stiffness etc. can be quickly investigated in a qualitative way without having the need to implement a completely new tyre data set. Scaling is done in such a way that realistic relationships are maintained. For instance, when changing the cornering stiffness and the friction coefficient in lateral direction (through λ_{Ky} and $\lambda_{\mu y}$), the abscissa of the pneumatic trail characteristic is changed in a way similar to that of the side force characteristic.

At the forthcoming second Tyre Colloquium to be held in Berlin, September 1996 a complete description of the new version of Delft Tyre will be presented including new dynamic features [6]. At TNO-WT (Delft, Fax: +31152697314) Delft Tyre commercial software is available.

TRANSIENT AND OSCILLATORY ASPECTS

Steady-state tyre models will loose their accuracy when the motion of the wheel shows variations in time. The fact that a deflection has to be built up to create a force calls for a model that contains carcass compliance. For the assessment of the side force and aligning torque response to varying slip angle and turn slip, a model based on the physical description of the lateral deflection of a stretched string restrained with respect to the wheel centre plane by an elastic foundation is often used. A portion of the string touches the ground. There, frictional forces are transmitted. Sliding is assumed not to occur, at least in the range close to the leading edge. We refer

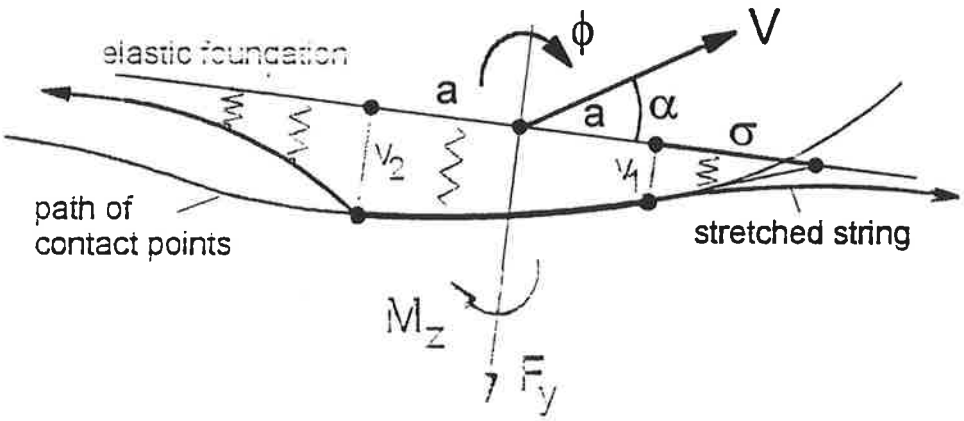

Figure 11 Stretched string tyre model for transient and oscillatory side force and moment response. The relaxation length σ has been indicated.

to [6] for details on the string model. Figure 11 depicts the deflected string model in top view. The input wheel motions are represented by the slip angle α and the turn slip ϕ. The latter quantity is the rate of change of the yaw angle with respect to travelled distance. In case the slip angle remains equal to zero, the turn slip equals the path curvature. The deflection of the string can be calculated in a rather simple manner starting from the leading edge (where sliding is assumed not to occur) until the transition point where sliding starts. For the deflection v_1 at the leading edge we have the following first-order ordinary differential equation:

$$\frac{1}{V_x}\frac{dv_1}{dt} + \frac{v_1}{\sigma} = \tan\alpha - a\phi \tag{19}$$

The symbol σ denotes the relaxation length and a stands for half the contact length. After multiplying left and right member with longitudinal wheel speed V_x and σ, neglecting turnslip ϕ and considering the possible presence of longitudinal slip (then V_x is to be replaced by the speed of rolling $V_r=V_x-V_{sx}$) we find (cf. Eq.(2)):

$$\sigma\frac{dv_1}{dt} + V_r v_1 = -\sigma V_{sy} \tag{20}$$

This version of differential equation (19) makes it possible to start and stop from and to stand-still ($V_r=V_x=0$). The prime effect of the differential equation is that a first-order lag of the output (the tyre deflection) with respect to the input (the wheel slip) arises. This lag is the main cause of e.g. the wheel shimmy phenomenon.

The slip quantities are assumed relatively small to allow the equation to be linear.Since it can be proven that the slope of the string deflection changes continuously around the leading edge (no kink), the string deflection angle α' in the foremost portion of the contact line directly relates to the deflection itself. We find:

$$\tan\alpha' = \frac{v_1}{\sigma} \tag{21}$$

At steady-state side slip conditions, this angle becomes equal to the slip angle α of the wheel. For not too small wavelengths of the motion, the curvature of the contact line may be neglected. Then, the string deflection will be approximately equal to the deflection that would arise at steady-state side slip with slip angle equal to the deflection angle calculated with Eq.(21). As a consequence, we may use the steady-state functions $F_y(\alpha')$ and $M_z(\alpha')$ according to e.g. the Magic Formula dealt with in the preceding section, to find the force and moment response to varying slip angle.

When operating in the larger range of slip the gradual decay of the relaxation length with increasing deflection angle is to be taken into account (cf. [8]). The response to turn slip becomes of importance at shorter wavelengths where for a better approximation the effect of a curved contact line should be taken into account. An equation similar to Eq.(20) can be derived for the response of the longitudinal deflection of the carcass to variations of the longitudinal wheel slip speed V_{sx}. A different relaxation length will then apply. A deformation gradient κ' may then be defined analogous to α'. From that gradient the longitudinal force $F_x(\kappa')$ is obtained. In case of time-varying combined slip, we may use the combined slip steady-state force and moment functions with α' and κ' used as the input slip quantities. Then, the two relaxation lengths showing decaying functions of both deflection gradients may be employed for greater accuracy (to be introduced in the next version of Delft Tyre).

Equation (20) holds for cases at limited levels of slip (still adhesion occurs near leading edge). However, the

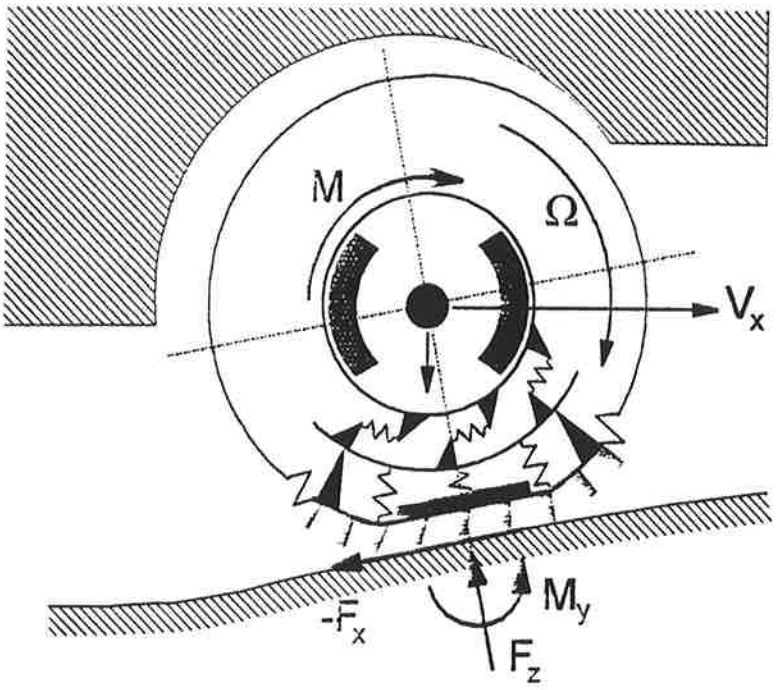

Figure 12 In-plane dynamic tyre/wheel model showing carcass tangential compliance.

model may still be used in cases where the slip increases to larger values. But when the slip is being reduced after having reached such high levels, an erroneous result may occur. This error may be avoided by using relaxation lengths depending on the deflection gradients according to [8]. Here the relaxation length (in (19) and (21)) is continuously adapted such that the lateral deflection v_l remains equal to the side force divided by the tyre lateral stiffness. Numerical difficulties may then be encountered at violent wheel oscillations. In [11] a solution to this problem is suggested. Cases of oscillating wheel motions at high levels of slip (e.g. situations where at violent

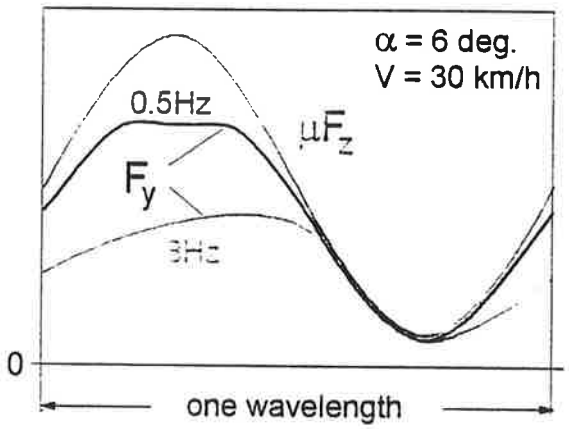

Figuur 13 Side force variation due to sinusoidal vertical wheel load fluctuations.

braking, ABS control gives rise to fluctuations of wheel slip) may call for a different model approach. In [9] a model is used in which the carcass fore and aft compliance is introduced explicitly. This implies that the relaxation length concept has been abandonded. In Figure 12 the model employed in [9] has been depicted. For reasons of computational causality a mass representing the lower portion of the tread band (belt) had to be included. The slip speed of that mass with respect to the road surface is then considered as input (via Eq.(1)) into the steady-state Magic Formula force model. Of course, the wheel/tyre polar moment of inertia has been included.

The differential equation (20) may also be used to study the effect of varying vertical load while cornering. Essential is then that the load dependency of the relaxation length $\sigma(F_z)$ is taken into account. Due to the gradient $\partial\sigma/\partial F_z$ a dynamic loss in average side force will occur when the side slipping wheel rolls over an undulated road surface. Figure 13 illustrates how F_y changes due to a sinusoidal variation of F_z while the wheel moves at a constant slip angle of 6 degrees. Two different frequencies have been considered. One very low (almost steady state) and the other relatively high. This simulated result shows a clear drop of the average side force at 8 Hz. In the diagram of Figure 14 the average loss in side force is presented as a function of frequency at three different amplitudes of the load variation. This loss should be minimized by (actively) controlling and limiting the variation of vertical load. It should then be realized that the effect is non-linear. Small to moderate amplitudes of the load will do no harm. Moreover, there is a wavelength effect (that is: more serious at shorter wavelengths, meaning: higher frequencies). Reference is made to [8] for further information.

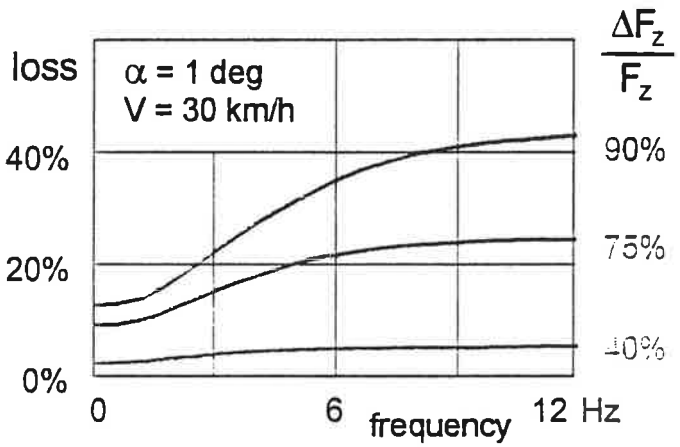

Figure 14 Static (at 0Hz) and dynamic loss in average side force at three amplitudes of vertical load fluctuations.

When higher frequencies, shorter wavelengths and/or high speeds are to be considered, the inclusion of tyre inertia and contact line curvature may become necessary. As the aligning torque is especially sensitive to inertia effects, Delft Tyre 96 takes the gyroscopic couple due to lateral tyre deformation rates into account, cf. [6, 7]. Figure 15 shows an example of theoretically assessed frequency response functions of the aligning torque to yaw oscillations (small angles, linear model with first belt vibrational modes considered [6]). The earlier mentioned phase lag can be seen to occur at relatively low values of speed and frequency. At higher speed the lag changes into a lead because of the effect of the gyroscopic couple that arises due to tilt angle variations of the belt with respect to the rim. A versatile tyre model for vehicle simulation studies is momentarily being developed in a project called SWIFT (Short Wavelength Intermediate Frequency Tyre model). In that model situations at (also large) combined slip are considered. Running over short unevennesses forms a difficult problem to model.

Effective road plane changes both in level and slope, and varying effective rolling radius (determined experimentally at very low speed) are employed as inputs to the relatively simple dynamic tyre model [10].

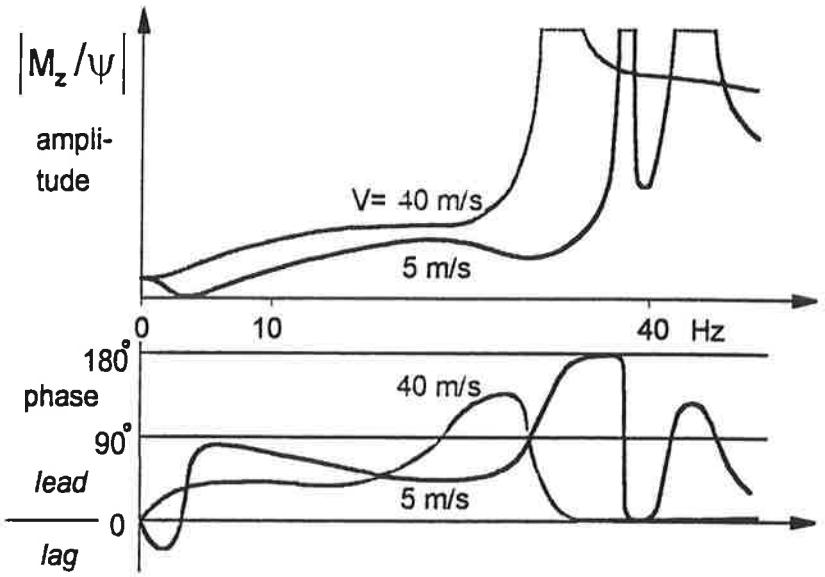

Figure 15 Aligning torque amplitude and phase frequency response to (small) steer angle variations according to a linear dynamic out-of-plane tyre model.

ACKNOWLEDGEMENTS

The development of Delft Tyre is a matter of continuous progress showing improvements in formulation and efficiency and widening of the dynamic range of operation. We much appreciate the enthusiastic involvement of students and staff of TU-Delft and TNO-WT. We owe special thanks to the students E. Branger and J. Koppenaal for their efforts in the improvement of the formulation of the aligning torque and to C.H. Verheul and J. van Oosten regarding the testing and implementation of the model. Also, P. van der Jagt (Goodyear) is thanked for his valuable advice connected with model reliability and adaptations to avoid computational difficulties.

REFERENCES

[1] H.B. Pacejka and R.S. Sharp, 'Shear force development by pneumatic tyres in steady state conditions: A review of modelling aspects'. Veh.Sys.Dyn. 20 (1991), pp. 121-176.

[2] W.R. Pasterkamp and H.B. Pacejka, 'On-line estimation of tyre characteristics for vehicle control'. AVEC '94, Japan, Oct. 1994.

[3] H.B. Pacejka and E. Bakker, 'The Magic Formula tyre model'. Proceedings 1st Tyre Colloquium, Delft, Oct.1991, Suppl. to Veh.Sys.Dyn., Vol. 21, 1993.

[4] J. van Oosten and E. Bakker, 'Determination of Magic Formula tyre model parameters'. Proceedings 1st Tyre Colloquium, Delft, Oct. 1991, Suppl. to Veh.Sys.Dyn., Vol. 21, 1993.

[5] P. Bayle, J.F. Forissier and S. Lafon, 'A new tyre model for vehicle dynamics simulations'. Automotive Technology International '93, pp. 193-198.
[6] H.B. Pacejka, 'In-plane and out-of-plane dynamics of pneumatic tyres'. Veh.Sys.Dyn. 10 (1981), pp. 221-251.
[7] H.B. Pacejka, 'A consistent Magic Formula tyre model with dynamic extension'. To be published in Proceedings of the "2nd Tyre Colloquium, Berlin, Sept.1996, Suppl. to Veh.Sys.Dyn.,1997.
[8] H.B. Pacejka and T. Takahashi, 'Pure slip characteristics of tyres on flat and on undulated road surfaces'. AVEC '92, Yokohama, Sept. 1992.
[9] P. van der Jagt, H.B. Pacejka and A.R. Savkoor, 'Influence of tyre and suspension dynamics on the braking performance of an anti-lock system on uneven roads'. EAEC Conf. '89, C382/047, IMechE 1989.
[10] P.W.A. Zegelaar and H.B. Pacejka, 'In-plane dynamics of tyres on uneven roads', Proceedings 14th IAVSD Symposium, Ann Arbor, Aug. 1995, Suppl. to Veh.Sys.Dyn., 1996.
[11] A. Higuchi and H.B. Pacejka, 'The relaxation length concept at large wheel slip and camber'. To be published in Proceedings of the "2nd Tyre Colloquium, Berlin, Sept.1996, Suppl. to Veh.Sys.Dyn.,1997.

APPENDIX Delft Tyre 96 (steady-state part)

The model is defined for positive longitudinal wheel speed ($V_x>0$, $-\frac{1}{2}\pi<\alpha<\frac{1}{2}\pi$). For negative forward speeds (running backwards) a mirror image approach may be used (as if the tyre runs forwards, cf. [7]). For the dynamic part we refer to [7].
Non-dimensional model parameters p, q, r and s have been introduced. For this we define: unloaded tyre radius R_o, nominal load F_{zo}, adapted nominal load $F'_{zo}=\lambda_{Fzo}F_{zo}$, normalized vertical load increment $df_z=(F_z-F'_{zo})/F'_{zo}$.

User Scaling Factors

For the user's convenience a set of scaling factors λ is available to examine the influence of changing a number of important overall parameters. The default value of these factors is set equal to one. We have:

pure slip

λ_{Fzo}	nominal (rated) load
$\lambda_{\mu x,y}$	peak friction coefficient
$\lambda_{Kx,y}$	slip stiffness (i.e. brake slip stiffness, cornering stiffness)
$\lambda_{Cx,y}$	shape factor
$\lambda_{Ex,y}$	curvature factor
$\lambda_{Hx,y}$	horizontal shift
$\lambda_{Vx,y}$	vertical shift
$\lambda_{\gamma y}$	camber force stiffness
$\lambda_{\gamma z}$	camber torque stiffness
λ_t	pneumatic trail (effecting aligning torque stiffness)
λ_{Mr}	residual torque

combined slip

$\lambda_{x\alpha}$	α influence on $F_x(\kappa)$
$\lambda_{y\kappa}$	κ influence on $F_y(\alpha)$
$\lambda_{Vy\kappa}$	κ induced 'ply-steer' F_y
λ_s	M_z moment arm of F_x

Longitudinal Force (pure longitudinal slip)

$$F_{xo} = D_x \sin[C_x \arctan\{B_x\kappa_x - E_x(B_x\kappa_x - \arctan(B_x\kappa_x))\}] + S_{Vx} \quad (22)$$

$$\kappa_x = \kappa + S_{Hx} \quad (23)$$

$$C_x = p_{Cx1} \cdot \lambda_{Cx} \qquad (>0) \quad (24)$$

$$D_x = \mu_x \cdot F_z \quad (25)$$

$$\mu_x = (p_{Dx1} + p_{Dx2} df_z) \cdot \lambda_{\mu x} \qquad (>0) \quad (26)$$

$$E_x = (p_{Ex1} + p_{Ex2} df_z + p_{Ex3} df_z^2) \cdot \{1 - p_{Ex4} \mathrm{sgn}(\kappa_x)\} \cdot \lambda_{Ex} \qquad (\le 1) \quad (27)$$

$$K_x = F_z \cdot (p_{Kx1} + p_{Kx2} df_z) \cdot \exp(-p_{Kx3} df_z) \cdot \lambda_{Kx} \quad \left(= B_x C_x D_x = \frac{\partial F_{xo}}{\partial \kappa_x} \text{ at } \kappa_x = 0\right) \quad (28)$$

$$B_x = K_x/(C_x D_x) \quad (29)$$

$$S_{Hx} = (p_{Hx1} + p_{Hx2} df_z) \cdot \lambda_{Hx} \quad (30)$$

$$S_{Vx} = F_z \cdot (p_{Vx1} + p_{Vx2} df_z) \cdot \lambda_{Vx} \cdot \lambda_{\mu x} \quad (31)$$

Lateral Force (pure side slip)

$$F_{yo} = D_y \sin[C_y \arctan\{B_y\alpha_y - E_y(B_y\alpha_y - \arctan(B_y\alpha_y))\}] + S_{Vy} \quad (32)$$

$$\alpha_y = \alpha + S_{Hy} \quad (33)$$

$$\gamma_y = \gamma \cdot \lambda_{\gamma y} \quad (34)$$

$$C_y = p_{Cy1} \cdot \lambda_{Cy} \qquad (>0) \quad (35)$$

$$D_y = \mu_y \cdot F_z \quad (36)$$

$$\mu_y = (p_{Dy1} + p_{Dy2} df_z) \cdot (1 - p_{Dy3} \gamma_y^2) \cdot \lambda_{\mu y} \qquad (>0) \quad (37)$$

$$E_y = (p_{Ey1} + p_{Ey2} df_z) \cdot \{1 - (p_{Ey3} + p_{Ey4} \gamma_y) \mathrm{sgn}(\alpha_y)\} \cdot \lambda_{Ey} \qquad (\le 1) \quad (38)$$

$$K_y = p_{Ky1} F_{zo} \sin[2 \arctan\{F_z/(p_{Ky2} F_{zo} \lambda_{Fzo})\}] \cdot (1 - p_{Ky3}|\gamma_y|) \cdot \lambda_{Fzo} \cdot \lambda_{Ky} \quad \left(= B_y C_y D_y = \frac{\partial F_{yo}}{\partial \alpha_y} \text{ at } \alpha_y = 0\right) \quad (39)$$

$$B_y = K_y/(C_y D_y) \quad (40)$$

$$S_{Hy} = (p_{Hy1} + p_{Hy2} df_z + p_{Hy3} \gamma_y) \cdot \lambda_{Hy} \quad (41)$$

$$S_{Vy} = F_z \cdot \{p_{Vy1} + p_{Vy2} df_z + (p_{Vy3} + p_{Vy4} df_z) \gamma_y\} \cdot \lambda_{Vy} \cdot \lambda_{\mu y} \quad (42)$$

Aligning Torque (pure side slip)

$$M_{zo} = -t \cdot F_{yo} + M_{zr} \tag{43}$$

$$t(\alpha_t) = D_t \cos[C_t \arctan\{B_t\alpha_t - E_t(B_t\alpha_t - \arctan(B_t\alpha_t))\}] \cdot \cos\alpha \tag{44}$$

$$\alpha_t = \alpha + S_{Ht} \tag{45}$$

$$M_{zr}(\alpha_r) = D_r \cos[\arctan(B_r\alpha_r)] \cdot \cos\alpha \tag{46}$$

$$\alpha_r = \alpha + S_{Hf} \quad (= \alpha_f) \tag{47}$$

$$S_{Hf} = S_{Hy} + S_{Vy}/K_y \tag{48}$$

$$\gamma_z = \gamma \cdot \lambda_{\gamma z} \tag{49}$$

$$B_t = (q_{Bz1} + q_{Bz2}df_z + q_{Bz3}df_z^2) \cdot (1 + q_{Bz4}\gamma_z + q_{Bz5}|\gamma_z|) \cdot \lambda_{Ky}/\lambda_{\mu y} \quad (>0) \tag{50}$$

$$C_t = q_{Cz1} \qquad (>0) \tag{51}$$

$$D_t = F_z \cdot (q_{Dz1} + q_{Dz2}df_z) \cdot (1 + q_{Dz3}\gamma_z + q_{Dz4}\gamma_z^2) \cdot (R_o/F_{zo}) \cdot \lambda_t \tag{52}$$

$$E_t = (q_{Ez1} + q_{Ez2}df_z + q_{Ez3}df_z^2) \cdot \{1 + (q_{Ez4} + q_{Ez5}\gamma_z)\arctan(B_tC_t\alpha_t)\} \quad (\le 1) \tag{53}$$

$$S_{Ht} = q_{Hz1} + q_{Hz2}df_z + (q_{Hz3} + q_{Hz4}df_z)\gamma_z \tag{54}$$

$$B_r = q_{Bz9}\lambda_{Ky}/\lambda_{\mu y} + q_{Bz10}B_yC_y \tag{55}$$

$$D_r = F_z \cdot \{q_{Dz6} + q_{Dz7}df_z + (q_{Dz8} + q_{Dz9}df_z)\gamma_z\} \cdot R_o \cdot \lambda_{Mr} \cdot \lambda_{\mu y} \tag{56}$$

Longitudinal Force (combined) (based on [5])

$$F_x = D_{x\alpha} \cos[C_{x\alpha} \arctan\{B_{x\alpha}(\alpha + S_{Hx\alpha})\}] \tag{57}$$

$$B_{x\alpha} = r_{Bx1} \cos[\arctan(r_{Bx2}\kappa)] \cdot \lambda_{x\alpha} \qquad (>0) \tag{58}$$

$$C_{x\alpha} = r_{Cx1} \qquad (>0) \tag{59}$$

$$D_{x\alpha} = F_{xo}/\cos[C_{x\alpha} \arctan(B_{x\alpha}S_{Hx\alpha})] \tag{60}$$

$$S_{Hx\alpha} = r_{Hx1} \tag{61}$$

Lateral Force (combined) (based on [5])

$$F_y = D_{y\kappa} \cos[C_{y\kappa} \arctan\{B_{y\kappa}(\kappa + S_{Hy\kappa})\}] + S_{Vy\kappa} \tag{62}$$

$$B_{y\kappa} = r_{By1} \cos[\arctan\{r_{By2}(\alpha - r_{By3})\}] \cdot \lambda_{y\kappa} \qquad (>0) \tag{63}$$

$$C_{y\kappa} = r_{Cy1} \qquad (>0) \tag{64}$$

$$D_{y\kappa} = F_{yo}/\cos[C_{y\kappa} \arctan(B_{y\kappa}S_{Hy\kappa})] \tag{65}$$

$$S_{Hy\kappa} = r_{Hy1} \qquad (< 0.1 \text{ (drive-slip)}) \tag{66}$$

$$S_{Vy\kappa} = D_{Vy\kappa} \sin[r_{Vy5} \arctan(r_{Vy6}\kappa)] \cdot \lambda_{Vy\kappa} \tag{67}$$

$$D_{Vy\kappa} = \mu_y F_z \cdot (r_{Vy1} + r_{Vy2}df_z + r_{Vy3}\gamma) \cdot \cos[\arctan(r_{Vy4}\alpha)] \tag{68}$$

Aligning Torque (combined)

$$M_z = -t \cdot F_y' + M_{zr} + s \cdot F_x \tag{69}$$

$$t = t(\alpha_{t,eq}) = D_t \cos[C_t \arctan\{B_t \alpha_{t,eq} - E_t(B_t \alpha_{t,eq} - \arctan(B_t \alpha_{t,eq}))\}] \cdot \cos\alpha \tag{70}$$

$$F_y' = F_y - S_{Vy\kappa} \tag{71}$$

$$M_{zr} = M_{zr}(\alpha_{r,eq}) = D_r \cos[\arctan(B_r \alpha_{r,eq})] \cdot \cos\alpha \tag{72}$$

$$s = \{s_{sz1} + s_{sz2}(F_y / F_{zo}) + (s_{sz3} + s_{sz4} df_z)\gamma\} \cdot R_o \cdot \lambda_s \tag{73}$$

$$\alpha_{t,eq} = \arctan\sqrt{\tan^2\alpha_t + \left(\frac{K_x}{K_y}\right)^2 \kappa^2} \cdot \mathrm{sgn}(\alpha_t) \tag{74}$$

$$\alpha_{r,eq} = \arctan\sqrt{\tan^2\alpha_r + \left(\frac{K_x}{K_y}\right)^2 \kappa^2} \cdot \mathrm{sgn}(\alpha_r) \tag{75}$$

Note: in expression (55) for B_r the second term has been recently introduced as a replacement of the first term; then, the suggested value for q_{Bz10} =1.5 and q_{Bz9} =0.